# Neutron, proton, and alpha emission in deep inelastic collisions of $^{16}O$ on three Ca isotopes at 102 and 142 MeV

S. Wald,* I. Tserruya, and Z. Fraenkel
*Department of Nuclear Physics, The Weizmann Institute of Science, Rehovot 76100, Israel*

G. Doukellis,† H. Gemmeke,‡ and H. L. Harney
*Max-Planck-Institut für Kernphysik, D-6900 Heidelberg, Federal Republic of Germany*
(Received 4 October 1982)

Energy and angular distributions of neutrons, protons, and alpha particles were measured in coincidence with the projectilelike fragment in deep inelastic collisions of $^{16}O$ on $^{40,44,48}Ca$ at 102 and 142 MeV. Using an event-by-event analysis which takes into account particle emission from both fragments and the recoil correction due to light particle emission, we show that our data are consistent with the assumption that the light particles are evaporated in the rest frame of the fragment accelerated projectilelike and targetlike fragments. This conclusion is based on the results for neutrons and alpha particles. But because of kinematic limitations which affect the alpha particle data, the conclusions based on the latter are less definitive.

NUCLEAR REACTIONS $^{40,44,48}Ca(^{16}O,X)$, $E=102$, 142 MeV, measured n, p, $\alpha$ in coincidence with projectilelike fragment; deduced c.m. energy spectra and multiplicities of the light particles. Results consistent with evaporation from the heavy fragments.

## I. INTRODUCTION

The angular and energy distributions of the neutrons, protons, and alpha particles emitted in coincidence with the heavy residues in a deep inelastic reaction (DIC) are considered to be an important tool for exploring the reaction mechanism. Schematically, we can distinguish two sources which can emit light particles (LP's): (i) the composite system formed during the short contact time and (ii) the heavy reaction products, i.e., the projectilelike and the targetlike fragments. In the second case the LP's may be emitted either before or after the fragment reaches its final velocity. Evaporation particles are emitted symmetrically around 90° in the center of mass (c.m.) system of the emitting source and have a Maxwellian energy spectrum. By measuring the angular and energy distribution of the LP's emitted in the interaction we can learn about the time of emission, the mechanism of emission, and also about the excitation energy of the heavy reaction products.

Investigations with "heavy" systems (projectile of $A \geq 32$) at energies below 10 MeV/nucleon have been made by measuring neutrons[1–7] and alpha particles[8] in coincidence with the heavy fragments. The results are consistent with a sequential process in which the excitation energy is shared among the products in proportion to their mass (or level densities), and the LP's are statistically emitted from the fully accelerated fragments. In $^{86}Kr+^{166}Er$ at 11.9 MeV/nucleon, Tserruya *et al.*[9] recently observed a small component of preequilibrium neutrons which appear in the quasielastic and the deeply inelastic energy regions.

In experiments with "light" systems (projectile of $A < 32$) at energies of 4–20 MeV/nucleon,[10–24] the angular distribution of the alpha particles was found to be sharply peaked around the beam direction,[12] the targetlike direction,[13] or the projectilelike direction.[18] Furthermore, three-body kinematic calculations seemed to show that all the possible emission processes are present. In some cases the LP's seem to chiefly originate from the targetlike product,[10] while in other cases it was claimed that the major source of LP's is the breakup of the projectilelike fragment (PF).[16] Finally, in some cases it was found that the LP's are emitted from the composite system.[12]

Recently, it was proposed that at least a part of the features which were thought to be a sign of preequilibrium emission of LP's could be due to kinematic effects which were not taken into consideration in the data analysis,[20–23] such as the influence of alpha particle emission by the projectilelike fragment on the angular correlation measured in the laboratory. Although the multiplicity of LP's from this fragment is relatively small, it has a strong effect on the angular distribution of the alpha particles due to the strong focusing by the fast projectilelike fragments. Furthermore, the alpha-particle mass is not negligible compared to the projectile mass (generally $^{12}C$ or $^{16}O$) and this causes an appreciable recoil of the projectilelike fragment by the LP emission. Since the heavy ion (HI) is observed after LP emission, its measured direction is different from its original one, and since the fragment angular distribution decreases nearly exponentially with increasing angle it is necessary to take into account this recoil effect. Hence, for calculating the LP multiplicity, one has to consider the heavy-ion angular distribution and use an exact expression for the laboratory to center-of-mass transformation. This point will be discussed later (Sec. III). Young *et al.*[23] measured the alpha particle emission in the bombardment of 204 MeV $^{16}O$ on $^{93}Nb$. They found that when the recoil effects are properly taken into account, the data are consistent with the alpha particles being evaporated from the heavy fragments after they

 

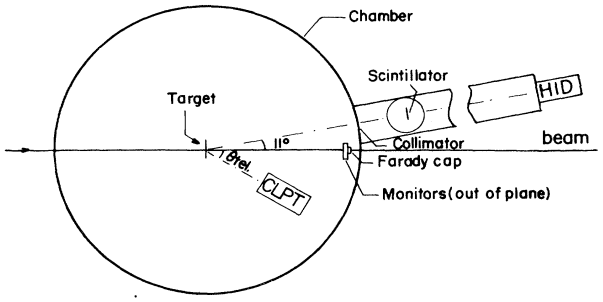


FIG. 1. The experimental setup in the WI experiment. HID is the heavy-ion ($dE$-$E$) detector. CLPT is the charged-light-particle telescope.

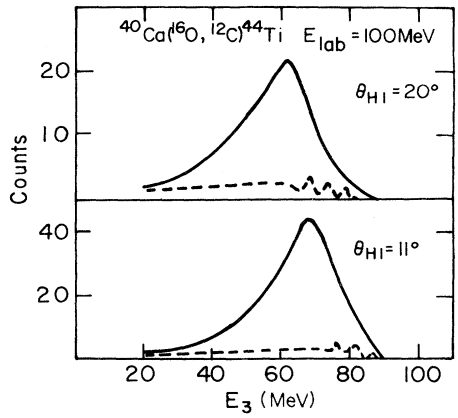


FIG. 2. PF singles energy spectrum at $\theta_{HI}=11°$ and 20° in the laboratory. The solid line is the yield of carbon measured from a $^{40}$Ca on a C backing. The dashed line is the contribution of the carbon backing. The absolute cross section of the carbon background was determined by the Na yield ratio of a pure-carbon target to that of the Ca target, as explained in Sec. II A.

reach their final velocity. However, for neutrons measured in the same system,[24] evidence of preequilibrium emission was found. The disagreement between the results of the different experiments and the contradicting interpretations motivated the present work.

In this experiment we measured neutrons, protons, and alpha particles in coincidence with the projectilelike fragment in the reaction of $^{16}$O with $^{40}$Ca, $^{44}$Ca, and $^{48}$Ca, at bombarding energies of 102 and 142 MeV. Information on all three LP's is necessary for a better estimate of the total excitation energy and its division between the fragments. The use of different target isotopes is important for identifying possible sources of preequilibrium LP emission. The multiplicity ratio of alpha to neutron emission should change drastically from $^{40}$Ca to $^{48}$Ca, if the emission occurs after thermal equilibrium is achieved. The measurement at two different energies should give additional information on the dependence of the preequilibrium emission on the beam energy, and how much of the excitation energy is carried away by this mechanism.

The experimental arrangement of the experiment is described in Sec. II. The data analysis is discussed in Sec. III. The experimental results are presented and discussed in Sec. IV. A summary is given in Sec. V. A preliminary report on the $^{16}$O+$^{48}$Ca results at 142 MeV is given in Ref. 25.

## II. THE MEASUREMENTS

We measured the angular correlation of the projectilelike fragment (PF) with neutrons (n), protons (p), and alpha particles ($\alpha$) in the bombardment of $^{16}$O on three Ca isotopes at two beam energies. Four sets of experiments were made. They are summarized in Table I. The measurement of $^{16}$O+$^{40}$Ca at 100 MeV was performed at the Weizmann Institute (WI) 14UD Pelletron accelerator. Only protons and alpha particles were measured in this experiment, which is described in Sec. II A. The other measurements were carried out at the MP tandem accelerator and post accelerator of the Max Planck Institut (MPI) für Kernphysik in Heidelberg. In these experiments we measured neutrons, protons, and alpha particles emitted in the reaction of 102 and 142 MeV $^{16}$O+$^{44}$Ca and 142 MeV $^{16}$O+$^{48}$Ca. The MPI experiments are described in Sec. II B. Calibration tests with $^{252}$Cf were done in order to extract the relative efficiency of the neutron detectors. These tests are discussed in Sec. II C.

### A. The WI 100 MeV $^{16}$O on $^{40}$Ca experiment

In this experiment we measured heavy ions (HI's) from carbon to neon in coincidence with protons and alphas.

TABLE I. Summary of the experimental systems.

| | 1st exp | 2nd exp | 3rd exp | 4th exp |
|---|---|---|---|---|
| Projectile and target | $^{16}$O, $^{40}$Ca | $^{16}$O, $^{44}$Ca | $^{16}$O, $^{44}$Ca | $^{16}$O, $^{48}$Ca |
| Bombarding energy (MeV) | 100 | 102 | 142 | 142 |
| $E_{c.m.}$-c.m. energy (MeV) | 71.4 | 74.8 | 104.1 | 106.5 |
| ($E_{c.m.}$-$V_{Coul}$) (MeV) | 45.9 | 49.8 | 79.2 | 81.9 |
| HI detector angle (deg) | 11° | 22° | 16° | 16° |
| Grazing angle: | | | | |
| $\theta_{lab}$ and $\theta_{c.m.}$ (deg) | 17.8, 24.8 | 16.8, 22.9 | 11.4, 15.5 | 11.1, 14.8 |
| Light particles detected | $p,\alpha$ | neutron, proton, alpha | | |
| Heavy-ion signals | $E,M,Z$ | $E$ and $Z$ | | |

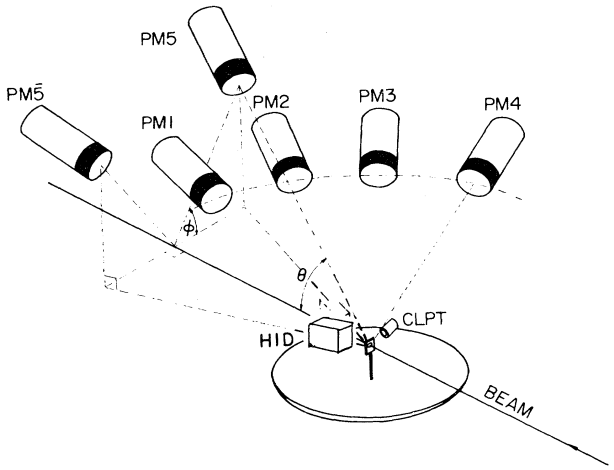


FIG. 3. The experimental setup of the MPI experiments. PM $n$ is the photomultiplier number $n$.

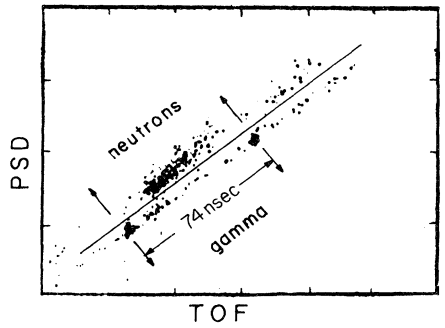


FIG. 4. An example of a pulse-shape discriminator (PSD) vs time-of-flight (TOF) plot for a neutron detector. The points below the line correspond to gamma events and those above it represent neutrons.

### *1. The experimental arrangement*

The charge, time of flight, and energy of the PF were measured with the experimental arrangement shown in Fig. 1. The HI detector was a *dE-E* telescope similar to that described in Ref. 26. The *dE* detector was an ionization chamber filled with isobutane at a pressure of about 20 Torr. The electric field between the grid and the collector was about 500 V/cm. The front window was a 300 $\mu$g/cm$^2$ Hostafan foil. The *E* detector was a 450 mm$^2$ silicon solid-state detector (SSD), with a depletion depth of 300 $\mu$m in which all the HI's were totally stopped. The *dE-E* telescope resolved charges ($Z$) of HI's between carbon and neon, and measured energies between 30 and 150 MeV, with a resolution better than 300 keV. The time of flight of the PF was also measured over a flight path of 122 cm between start pulses from a 150 $\mu$g/cm$^2$ scintillation foil and stop pulses from the *E* detector. The time resolution was about 350 psec. The mass of the heavy ion was determined from the time of flight and the energy. The mass resolution was better than 5% in the carbon-

TABLE II. Location of the detector in all experiments. 1st experiment, $^{16}$O + $^{40}$Ca at 100 MeV; 2nd experiment, $^{16}$O + $^{44}$Ca at 102 MeV; 3rd experiment, $^{16}$O + $^{44}$Ca at 142 MeV; and 4th experiment, $^{16}$O + $^{48}$Ca at 142 MeV. $\theta$ and $\phi$ are the polar and azimuthal laboratory angles (in degrees), respectively. The HI detector location is defined by the polar angle $\theta_{HI}$ and its azimuthal angle is $\phi_{HI}=180°$. The top part of the table gives the location of the charged light particle telescope (CLPT). The bottom part of the table gives the location of the neutron counters in all experiments. The locations in parentheses refer to the geometry we obtained by moving the HI detector to $\phi_{HI}=0°$ and leaving the neutron detectors fixed in their positions.

| | $\theta_{HI}$ | | CLPT positions | | | | | | | | | | | | |
|---|---|---|---|---|---|---|---|---|---|---|---|---|---|---|---|
| | | | 1 | 2 | 3 | 4 | 5 | 6 | 7 | 8 | 9 | 10 | 11 | 12 | 13 |
| 1st exp | 11° | $\theta$ | 20 | 30 | 40 | 50 | 60 | 27 | 37 | 47 | 28 | 35.5 | | | |
| | | $\phi$ | 0 | 0 | 0 | 0 | 0 | 180 | 180 | 180 | 46.8 | 59.4 | | | |
| 2nd exp | 22° | $\theta$ | 30 | 35 | 45 | 60 | 40 | 50 | 60 | | | | | | |
| | | $\phi$ | 0 | 0 | 0 | 0 | 180 | 180 | 180 | | | | | | |
| 3rd exp | 16° | $\theta$ | 15 | 20 | 30 | 40 | 50 | 60 | 70 | 33 | 40 | 58 | 35.5 | 41.4 | 48.4 |
| | | $\phi$ | 0 | 0 | 0 | 0 | 0 | 0 | 0 | 180 | 180 | 180 | 59.4 | 49.1 | 41.9 |
| 4th exp | 16° | $\theta$ | 15 | 20 | 30 | 40 | 50 | 60 | 70 | 33 | 40 | 60 | | | |
| | | $\phi$ | 0 | 0 | 0 | 0 | 0 | 0 | 0 | 180 | 180 | 180 | | | |

| | $\theta_{HI}$ | | PM positions | | | | | |
|---|---|---|---|---|---|---|---|---|
| | | | 1 ($\bar{1}$) | 2 ($\bar{2}$) | 3 ($\bar{3}$) | 4 ($\bar{4}$) | 5 ($\bar{5}$) | $\bar{5}$ (5) |
| 2nd exp | 22° | $\theta$ | 17 | 32 | 65 | 85 | 35.5 | 35.5 |
| | | $\phi$ | 0 (180) | 0 (180) | 0 (180) | 0 (180) | 59.4 (120.6) | 120.6 (59.4) |
| 3rd and 4th exp's | 16° | $\theta$ | 17 | 32 | 47 | 65 | 35.5 | 35.5 |
| | | $\phi$ | 0 (180) | 0 (180) | 0 (180) | 0 (180) | 59.4 (120.6) | 120.6 (59.4) |

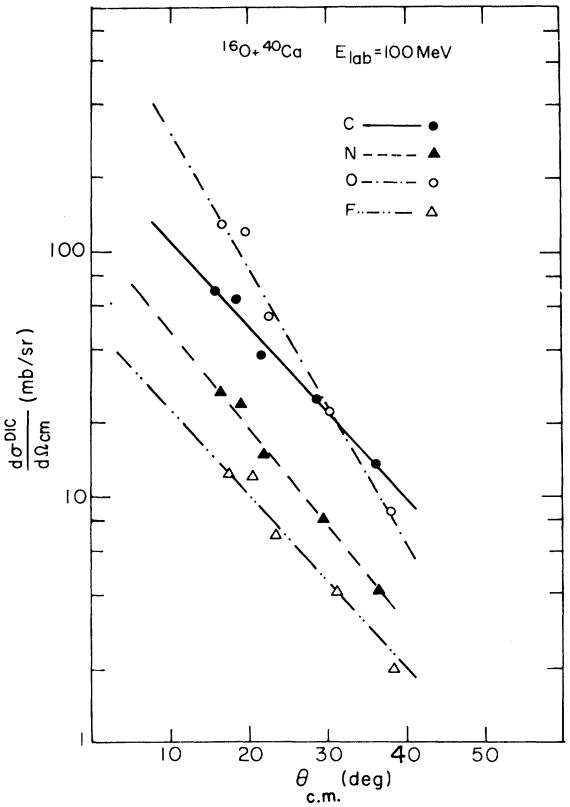


FIG. 5. The angular distribution in the center of mass of various Z of the PF in $^{16}O + ^{40}Ca$ at 100 MeV, integrated over the PF laboratory energy range between 35 and 85 MeV.

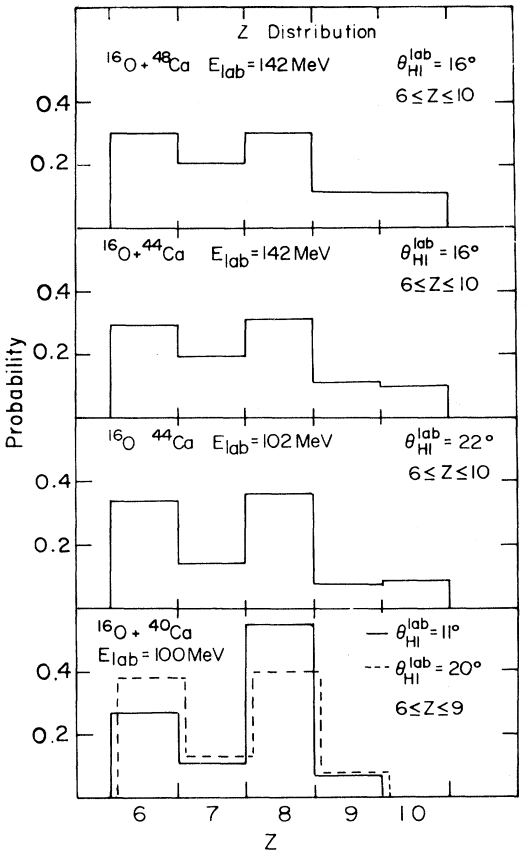


FIG. 6. Charge distribution in all the experiments.

neon region. The solid angle covered by the HI detector was $13\times10^{-3}$ msr. The charged light particles (CLP's) were measured with a telescope consisting of three SSD's of 18 $\mu$m ($T1$), 200 $\mu$m ($T2$), and 2000 $\mu$m ($T3$) thickness. Detector $T1$ was used as a $dE$ detector and $T2$ as an $E$ detector to identify alpha particles up to 20 MeV. For higher energies both $T1$ and $T2$ served as a $dE$ detector and $T3$ as an $E$ detector. The upper energy limit was 40 MeV for the alpha particles and 18 MeV for protons, since particles above this energy were not totally stopped in $T3$. The lower energy cutoff was 5 MeV for alpha particles and 1 MeV for protons due to the thickness of the $T1$ detector. It was possible to move the telescope in and out of the reaction plane. The LP telescope was 5.5 cm from the target and covered a solid angle of 2.3 msr. Two 300 $\mu$m Si 150 mm$^2$ SSD's were placed at $\pm15°$, above and below the reaction plane, with a solid angle of 60 $\mu$sr. These detectors were used as monitors.

The target was about 300 $\mu$g/cm$^2$ of 99.96% $^{40}$Ca on a 20 $\mu$g/cm$^2$ carbon backing. The target was transferred under vacuum to the chamber to avoid oxidation.

Every LP-PF coincidence event and about 5% of the single PF events were recorded. The data were accumulated event by event on magnetic tape via a PDP-9 computer.

TABLE III. Average $Q$ value, as measured from all the HI spectra in the various experiments (second column). The numbers in parentheses indicate the width of the $Q$-value distribution. Also shown are (a) $T$, the temperature derived from the slope of the neutron c.m. energy spectra, (b) $aT^2$, with $a = A/10$ ($A$ is the mass number), and (c) the excitation energies calculated with formula (4.3) using the measured multiplicities and average LP energies. The errors in the temperature values are about 30%. $T$, $aT^2$, $Q$, and $E^*$ are in MeV.

| Experiment number | $\theta_{HI}$ | $\bar{Q}$ (MeV) | PF $T$ | PF $aT^2$ | PF $E^*_{PF}$ | TF $T$ | TF $aT^2$ | TF $E^*_{TF}$ |
|---|---|---|---|---|---|---|---|---|
| 1 | 11° | −30.6 (9.8) | | | | | | |
| | 20° | −31.2 (10.6) | | | | | | |
| 2 | 22° | −32.2 (15.1) | 1.8 | 5. | 2.9±2.0 | 2.3 | 28. | 34.0±10.5 |
| 3 | 16° | −66.2 (21.0) | 2.2 | 8. | 10.3±4.9 | 3.8 | 61. | 61.3±17.2 |
| 4 | 16° | −65.8 (21.0) | 2.2 | 8. | 9.5±4.3 | 3.7 | 60. | 60.2±15.1 |

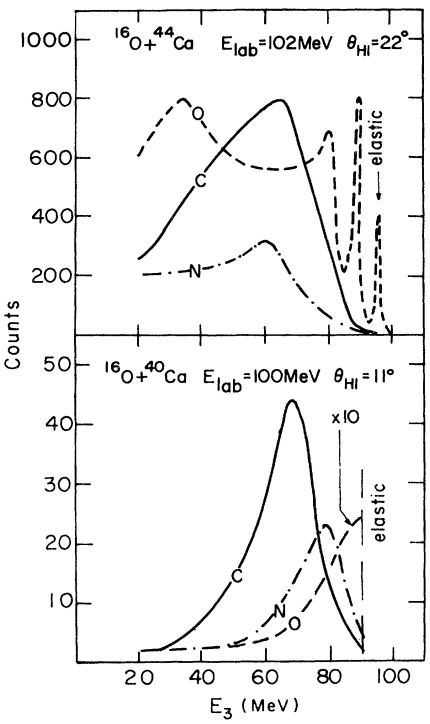


FIG. 7. Laboratory energy spectra for carbon, nitrogen, and oxygen in the $^{16}O + ^{40}Ca$ at 100 MeV and $^{16}O + ^{44}Ca$ at 102 MeV experiments. The spectra are smoothed over a 2.5 MeV interval.

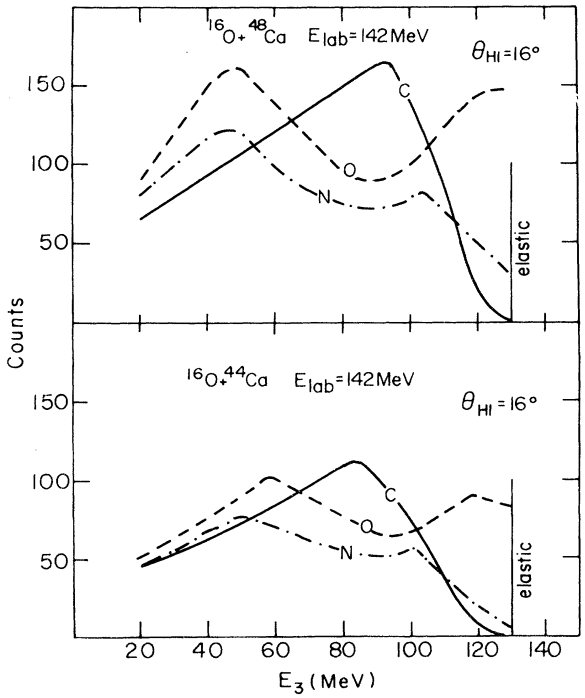


FIG. 8. Laboratory energy spectra for carbon, nitrogen, and oxygen in $^{16}O + ^{44}Ca$ and $^{16}O + ^{48}Ca$ at 142 MeV experiments. The spectra are smoothed over 2.5 MeV.

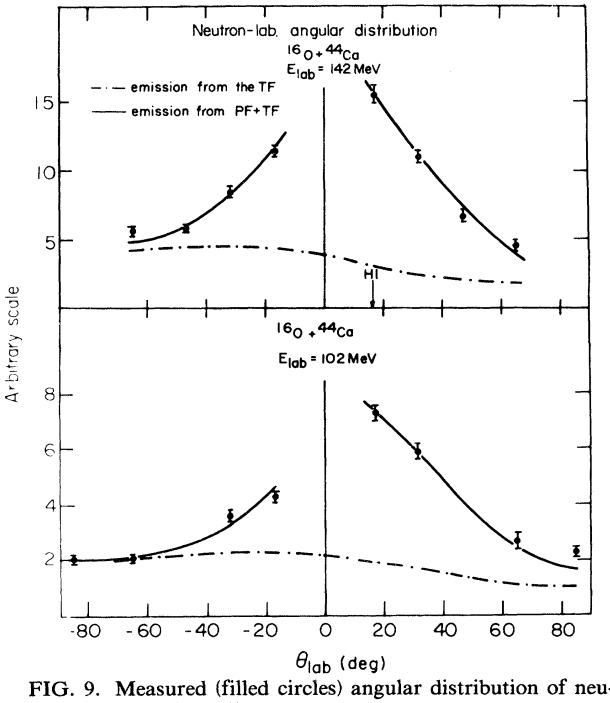


FIG. 9. Measured (filled circles) angular distribution of neutrons emitted in $^{16}O + ^{44}Ca$ at 102 and 142 MeV. The solid line is the calculated neutron angular distribution. The calculated contribution of the neutrons emitted by TF is given by the dotted-dashed line. HI denotes the angle of the heavy ion detector.

### 2. *The experiment*

The angular distribution of the PF was measured between 11° and 25°. The same measurements were also done with a Ca + Au target in order to determine the thickness of the Ca target. Measurements were done with a pure C target in order to determine the contribution of the C backing in both the singles and the coincidence yields. This contribution could not be determined by normalizing the elastic scattering peak of $^{16}O + ^{12}C$, since it was located in the tail of the strong elastic peak of $^{16}O + ^{40}Ca$. Instead we used the marked difference in the isotope yield of the two targets, particularly for Na, i.e., we assumed that the Na yield of both targets originate solely from the C. This procedure gives an upper limit of the C contribution. The normalized $^{12}C$ energy spectra[10] obtained with the $^{40}Ca$ and $^{12}C$ targets are shown in Fig. 2. It is seen that the C contribution in the singles yield of C is negligible (less than 10% at $\theta_{HI}=11°$). Its contribution was even smaller for the singles yield of the other isotopes and also for the coincidence yield with all isotopes. Most of the $\alpha$-C coincidence yield with the C target occurred at low energies ($E<20$ MeV) of the PF; we therefore restricted the analysis to PF's with energies $E>20$ MeV (see Sec. IV). We found that with this procedure the upper limit of the C contribution to the $\alpha$-coincidence yield is about 3%. The same limits apply to the measurements of $^{16}O + ^{44}Ca$ at 102 MeV. Owing to this very low contribution of the C contaminant we did not perform a separate measurement with a C target at the higher bombarding energy of 142 MeV. The relative yield of Na at this energy was also

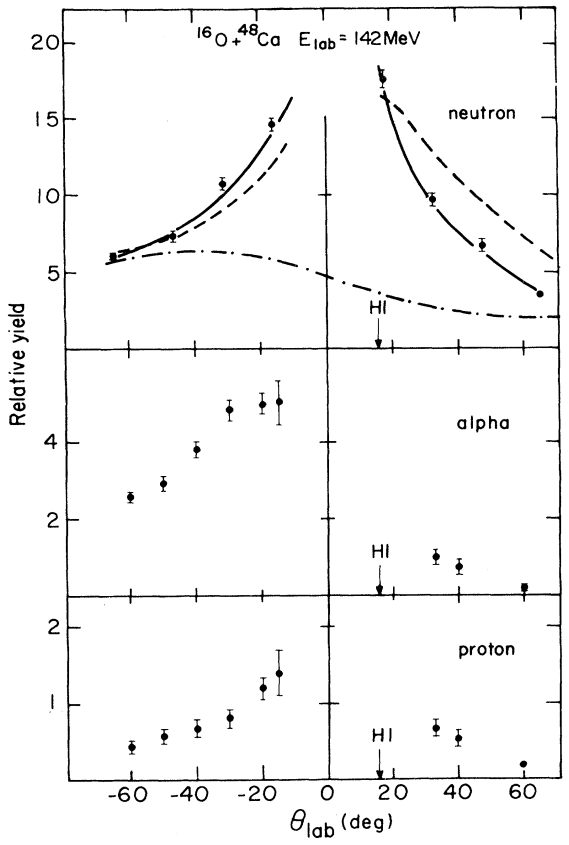


FIG. 10. Measured (filled circles) angular distribution of neutrons, alpha particles, and protons emitted in $^{16}O + ^{48}Ca$ at 142 MeV. The solid line is the calculated neutron angular distribution. The calculated contribution of the neutrons emitted by TF is given by the dotted-dashed line. The dashed line denotes the calculated neutron angular distribution without the recoil correction (see text). HI denotes the angle of the heavy ion detector.

very small. However, for the reasons stated above, we restricted the analysis of the 142 MeV data to PF's with energies $E > 25$ MeV. We estimate that the C contribution at the higher bombarding energy is $< 10\%$. During the coincidence measurements the PF detector was at a fixed laboratory angle of 11°. The LP telescope was moved to different angles in and out of the reaction plane (see the top portion of Table II).

Up to 300 alpha particles and 40 protons were measured for each position of the LP telescope in coincidence with HI in the DIC region (PF energy between 35 and 85 MeV). Random coincidence events accounted for 1—4 % of the total coincidence yield.

### B. MPI 102, 142 MeV $^{16}O+^{44}Ca$, $^{48}Ca$ experiments

In these experiments we measured neutrons, protons, and alpha particles in coincidence with the PF. The 102 MeV experiment was done with the MP tandem accelerator operating in a pulsed mode and the 142 MeV experiments with the MP tandem plus the post accelerator.

#### *1. The experimental arrangement*

The experimental setup is shown in Fig. 3. The charge and energy of the PF were determined in this experiment. The PF detector and the LP telescope were the ones used in the WI experiment. They covered solid angles of 4.6 and 1.6 msr, respectively. Two monitor detectors were located at ±20° to the beam in the reaction plane.

Neutrons were detected in six NE-213 liquid scintillators, 5.1 cm thick and 11.3 and 12.6 cm in diameter. The liquid scintillators enabled neutron-gamma pulse shape discrimination. The electronic threshold of the photomultipliers (PM's) was adjusted to correspond to neutrons of 200 keV. The PM's were at a distance of 80 cm from the target and covered a solid angle of 15 msr.

From each particle detected in the neutron counters, we recorded three signals: (1) the time signal from the anode;

TABLE IV. Average multiplicity $\nu_{PF(TF)}$ and average c.m. energy $E_{PF(TF)}$ (MeV) of neutrons, alpha particles, and protons emitted from the PF (TF) in all experiments. The data were averaged over $Z=6-10$ for neutrons and $Z=6-8$ for alpha particles and protons. The DIC energy range was chosen to be TKE=25—85 MeV for the 142 MeV experiments and TKE=20—60 MeV for the 100 and 102 MeV experiments. The errors indicated are statistical, the systematic errors are estimated to be ~20%.

| Exp | LP | $\bar{\nu}_{PF}$ | $\bar{E}_{PF}$ | $\bar{\nu}_{TF}$ | $\bar{E}_{TF}$ |
|---|---|---|---|---|---|
| $^{16}O + ^{40}Ca$ | | | | | |
| at | alpha | | | 0.9 ±0.2 | |
| 100 MeV | proton | | | 0.6 ±0.2 | |
| $^{16}O + ^{44}Ca$ | neutron | 0.05±0.01 | 1.7±0.5 | 0.15±0.02 | 2.7±0.7 |
| at | alpha | 0.02±0.03 | 4.5±3.2 | 0.9 ±0.2 | 9.2±2.4 |
| 102 MeV | proton | 0.08±0.01 | 2.7±1.6 | 0.35±0.11 | 6.3±2.6 |
| $^{16}O + ^{44}Ca$ | neutron | 0.19±0.02 | 2.3±0.8 | 0.76±0.05 | 3.6±0.4 |
| at | alpha | 0.11±0.01 | 5.2±0.4 | 1.6 ±0.3 | 8.5±1.5 |
| 142 MeV | proton | 0.29±0.03 | 4.3±0.7 | 0.4 ±0.1 | 7.7±3.4 |
| $^{16}O + ^{48}Ca$ | neutron | 0.22±0.02 | 2.5±0.6 | 1.25±0.06 | 3.7±0.4 |
| at | alpha | 0.12±0.02 | 5.3±0.6 | 1.6 ±0.5 | 9.2±1.8 |
| 142 MeV | proton | 0.20±0.06 | 4.4±1.5 | 0.3 ±0.1 | 4.9±3.3 |

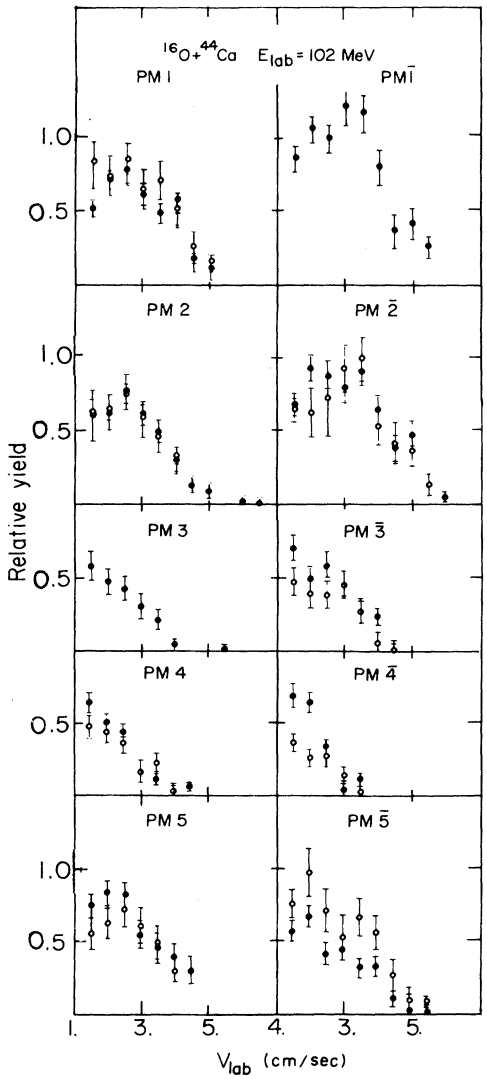


FIG. 11. Measured (filled circles) neutron laboratory velocity spectra compared with projected (open circles) spectra obtained from the reference counters PM $\bar{1}$ and PM 3 in $^{16}O + ^{44}Ca$ at 102 MeV.

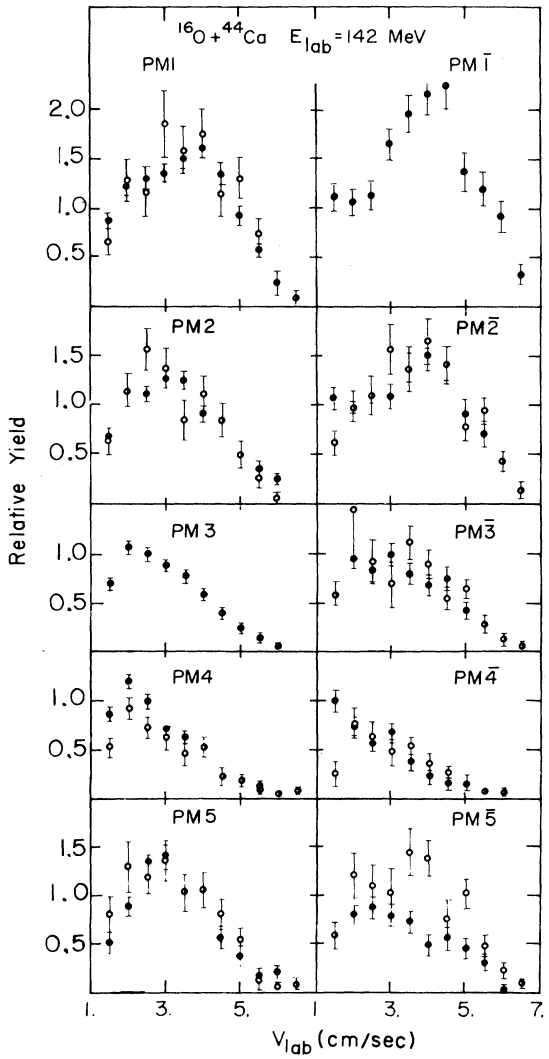


FIG. 12. Measured (filled circles) neutron laboratory velocity spectra compared with projected (open circles) spectra obtained from the reference counters PM $\bar{1}$ and PM 3 in $^{16}O + ^{44}Ca$ at 142 MeV.

(2) the energy signal from the last dynode, used for efficiency calculations (see Sec. II C); and (3) the pulse-shape signal used for neutron-gamma discrimination.

The gamma-neutron discrimination was carried out using the time of flight and the pulse-shape discriminator signals in each event. The plot of time of flight versus pulse shape (Fig. 4) shows a clear separation between gammas and neutrons.

The scattering chamber was made of 3 mm thick aluminum and was 60 cm in diameter. The thin walls reduce the neutron and gamma background which originated chiefly from (n,n'$\gamma$) and (n,$\gamma$) processes in the chamber walls. The Faraday cup was a few meters from the chamber and was well shielded.

The targets were $\sim$300 $\mu$g/cm$^2$ of 98.55% $^{44}$Ca or 97.16% $^{48}$Ca on a 20 $\mu$g/cm$^2$ carbon backing. They were transferred under vacuum to the chamber to avoid oxidation.

The accelerator was run in a pulsed-beam mode. The time interval between two successive pulses was 74 nsec, with a time resolution better than 0.4 nsec. The pulses from the pulsing system of the accelerator were used as a reference (start signal) for the neutron time-of-flight measurements. The range of the TDC was 200 nsec, so that three beam bursts could be observed and random coincidences could be corrected for.

As in the WI experiment, we recorded every LP (CLP or neutrons) HI coincidence and a fraction of the heavy ion singles. The data were recorded event by event on magnetic tape, via CAMAC logic and a PDP 11/34 computer.

### 2. *The experiments*

The different measurements and the angles of the detectors are listed in Tables I and II. Four PM's were located

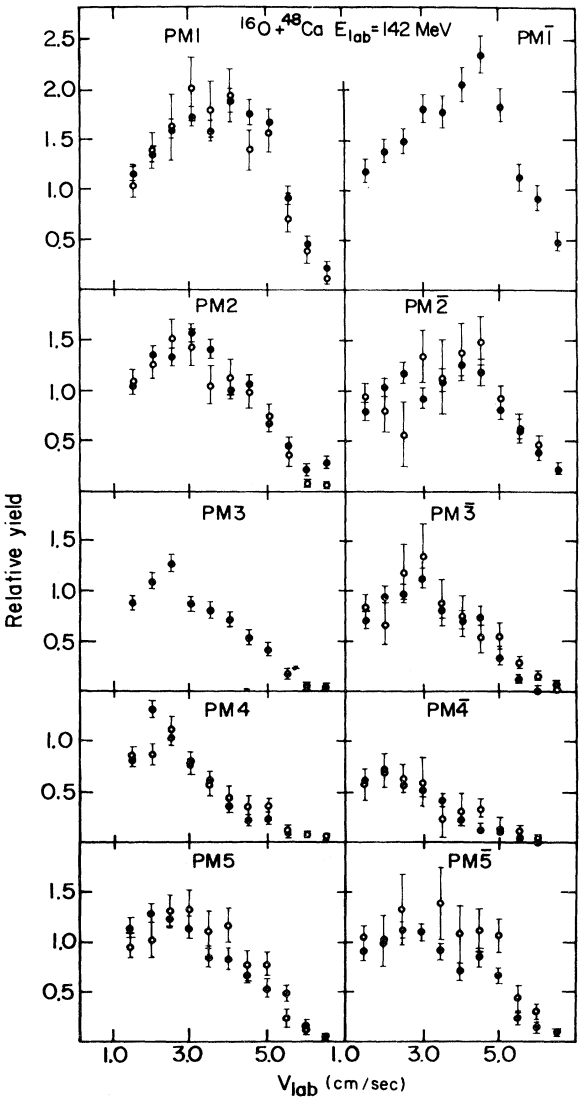


FIG. 13. Measured (filled circles) neutron laboratory velocity spectra compared with projected (open circles) spectra obtained from the reference counters PM $\bar{1}$ and PM 3 in $^{16}O + ^{48}Ca$ at 142 MeV.

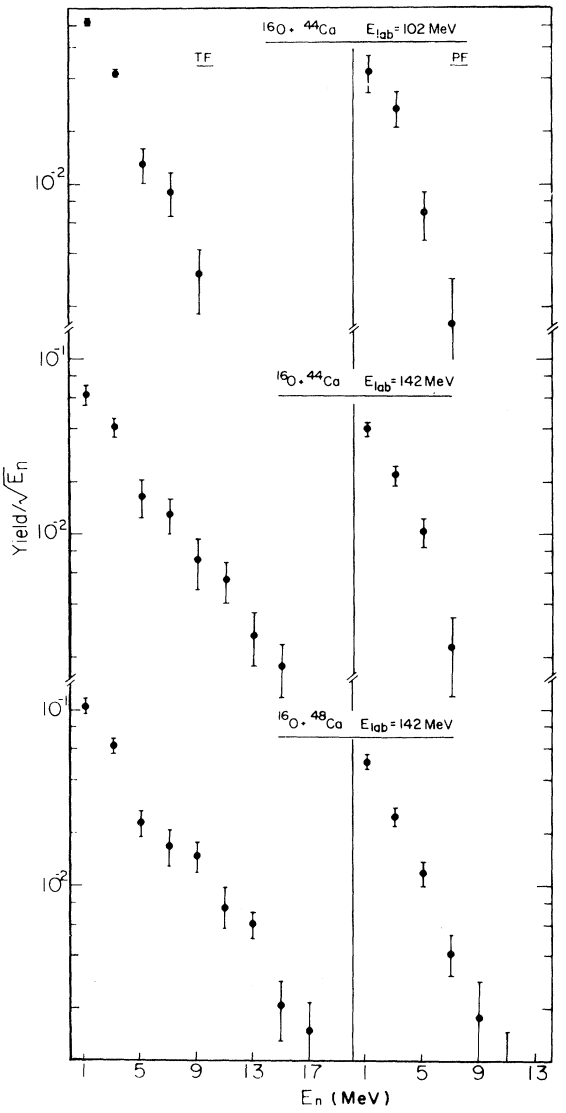


FIG. 14. The c.m. energy distribution of neutrons emitted by the PF and TF. The data points were obtained using the reference counters as indicated in Figs. 11—13.

*in* the reaction plane and on the *same* side with respect to the beam. Two out-of-plane PM's were located symmetrically with respect to the beam axis (see Fig. 3). During each run we moved the PF detector from one side of the beam to the other side in the same plane, keeping the same angle with respect to the beam. Using this method we doubled the number of relative angles between the PF and the neutron counters.

On the average about $10^7$—$10^8$ PF's were detected in every experiment. About 5% of the noncoincidence events were recorded on the magnetic tape. About 400—1000 alpha-coincidence events and about 100 proton-coincidence events were detected for each CLP telescope position, while about 2500 neutrons were measured in each PM for each of the two heavy ion detector (HID) positions, of which 10% were random events.

### C. Calibration of the neutron detectors

In order to measure the neutron absorption due to the HI detector and the CLP telescope, a $^{252}Cf$ source attached to a 450 mm$^2$ SSD was mounted on the target holder. One fission fragment was measured in coincidence with the neutrons, and the start pulse for the neutron time of flight was taken from the fission fragment detector. The neutron multiplicity (the ratio of the number of neutrons to the number of fission fragments) as a function of neutron energy was measured for each PM, for various positions of the HI detector, the CLP telescope, and neighboring PM's. In this way we obtained absorption factors for each detector for every geometrical arrangement of the experiments.

The efficiency of the neutron detectors as a function of

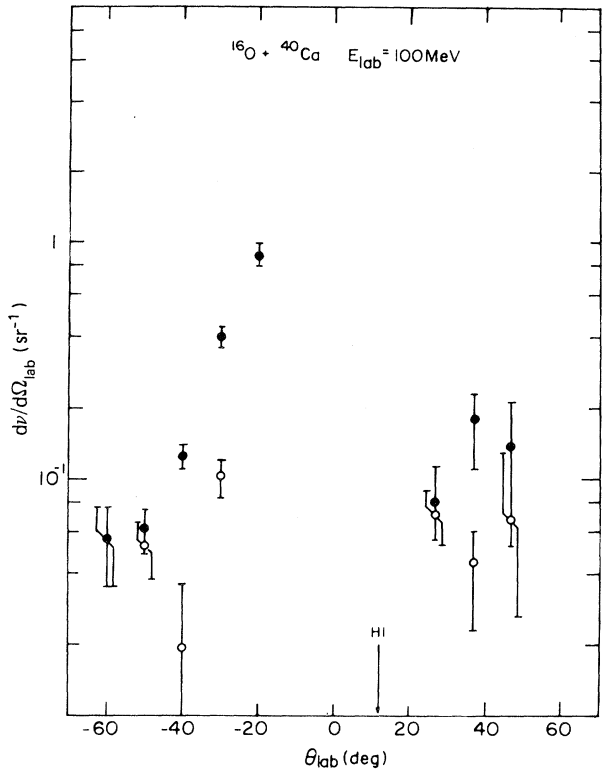


FIG. 15. Differential multiplicity $d\nu/d\Omega_{lab}$ for alpha particles (filled circles) and protons (open circles) in the laboratory for $^{40}Ca(^{16}O,^{12}C)$ at 100 MeV.

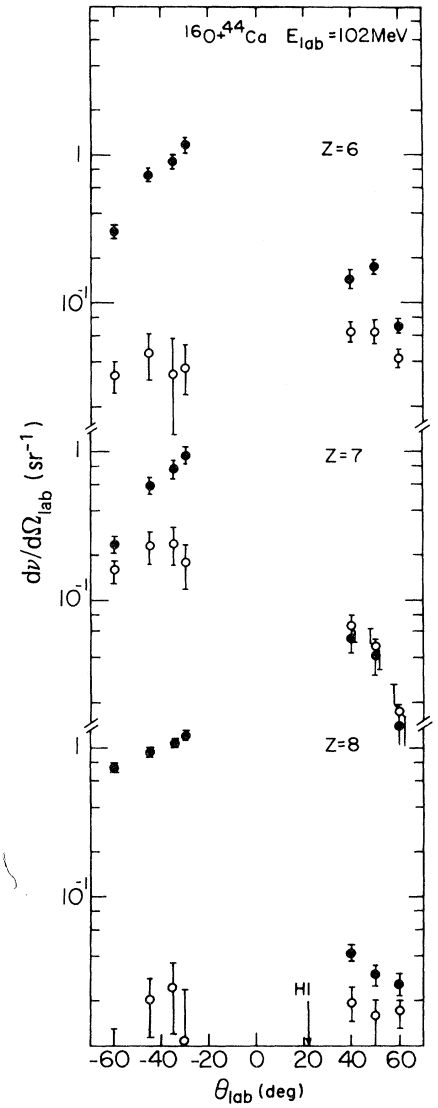


FIG. 16. Differential multiplicity $d\nu/d\Omega_{lab}$ for alpha particles (filled circles) and protons (open circles) in the laboratory for carbon, nitrogen, and oxygen projectilelike fragments in $^{16}O + ^{44}Ca$ at 102 MeV.

neutron energy was calculated using the method of Drosg.[27] To use this scheme, one has to calibrate the pulse height from the PM with respect to the recoiling proton energy in the scintillator. This was done for the $^{252}Cf$ runs by putting windows on a few neutron energies and looking for the high energy edge in the corresponding pulse height spectra. This calibration was compared to a calibration made using gamma sources. The Compton edges of $^{54}Mn$, $^{137}Cs$, $^{22}Na$, and $^{60}Co$ in the pulse height spectra defined the calibration of the pulse height against the recoiling electron energy in a $(\gamma,e)$ process. The energy calibration of electrons with respect to the actual energy of the protons is known in a limited energy range.[27] In this range both methods were in agreement.

The efficiencies were calculated for a threshold of 1 MeV neutrons. We therefore disregarded in the off-line data analysis all events with pulse height lower than that value. To check the stability of all calibrations the $^{252}Cf$ tests were repeated after each beam time, and thresholds of the PM's were checked periodically during the runs.

## III. DATA ANALYSIS

A detailed description of the method used for the data analysis is given in Ref. 28. Our data analysis is based on the assumption that LP's are evaporated isotropically in the rest frame of the fully accelerated fragments. With this assumption, the LP velocity spectra in the rest frame of the PF and TF (c.m. spectra) can be obtained from the laboratory spectra of only *two* out of the ten locations of the neutron detectors. These two detectors (which were the ones closest to the direction of the PF and TF) will be referred to as reference counters. The c.m. velocity spectra (obtained from the two reference counters) were projected back into the laboratory system at angles corresponding to the other neutron detectors. The projected spectra so obtained were compared with the experimental ones. Agreement between the two sets of spectra shows the experimental results to be compatible with our initial assumption. A similar procedure was used for the analysis of the proton and alpha particle results (see below). In the laboratory—to—center-of-mass transformation, we used the exact Jacobian which took into account the recoil of the PF due to LP emission.[28] In order to car-

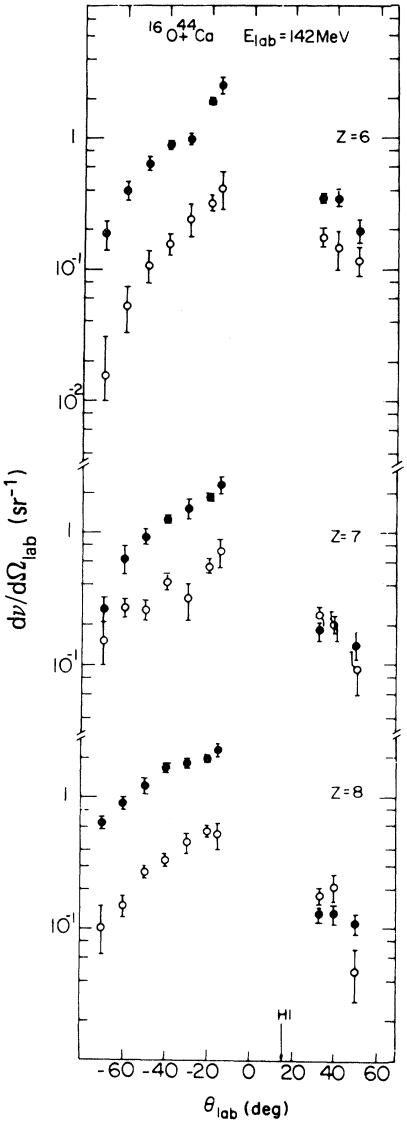


FIG. 17. Differential multiplicity $d\nu/d\Omega_{lab}$ for alpha particles (filled circles) and protons (open circles) in the laboratory for carbon, nitrogen, and oxygen in $^{16}O + ^{44}Ca$ at 142 MeV.

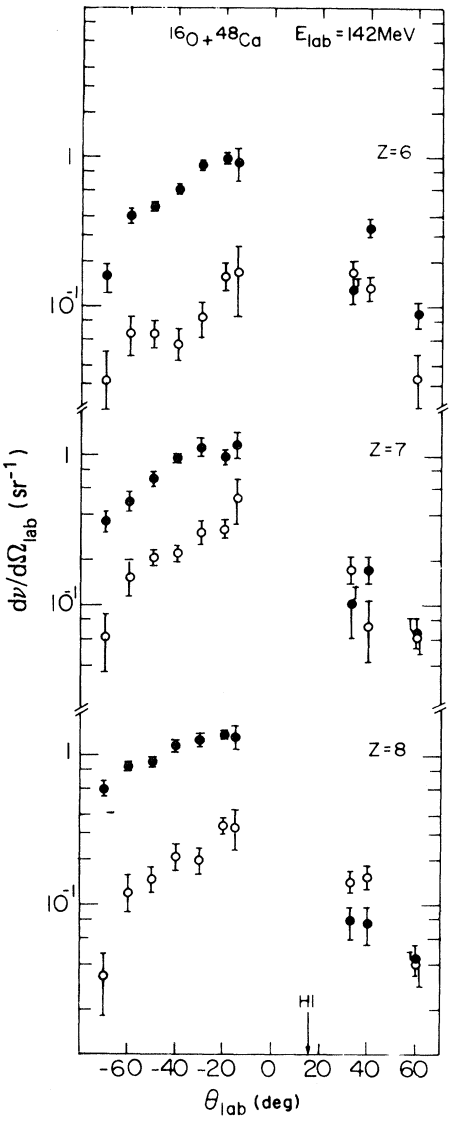


FIG. 18. Differential multiplicity $d\nu/d\Omega_{lab}$ for alpha particles (filled circles) and protons (open circles) in the laboratory for carbon, nitrogen, and oxygen in $^{16}O + ^{48}Ca$ at 142 MeV.

ry out the calculations we had to make two more assumptions. For each event we chose for the final PF mass the most probable one for the measured $Z$ (as obtained in the $^{16}O+^{40}Ca$ experiment). The second assumption concerns the initial PF c.m. angular distribution. The differential cross sections in the c.m., for elements between C and F, are given in Fig. 5 for $^{16}O$ on $^{40}Ca$ at 100 MeV. In the other experiments, the angular distribution of the PF was not measured and therefore we had to assume a certain initial PF angular distribution in the c.m. Since the cross sections in Fig. 13 exhibit an exponential behavior similar to those observed in other systems, we parametrized the angular distribution of the PF by the following expression[29]:

$$\frac{d\sigma}{d\Omega_{c.m.}} \propto \frac{1}{\sin\theta_{c.m.}} \exp(-\theta_{c.m.}/\Delta\theta) \ . \tag{3.1}$$

For the narrow range of PF angles which is of interest in the present experiment, we further assumed that the $Z$ (or mass) and total kinetic energy (TKE) distributions were independent of angle. The average $\Delta\theta$ for all $Z$'s from C to O in the $^{16}O+^{40}Ca$ experiment was $\Delta\theta=22°$ and the same value $\Delta\theta=22°$ was used for the $^{16}O+^{44}Ca$ at 102 MeV data. For the experiments at 142 MeV $^{16}O$ on $^{44}Ca$ and $^{48}Ca$ we assumed $\Delta\theta=8°$, which yields a reasonable fit of the neutron data of both experiments. The choice of this parameter was made by trial and error and no best-fit procedure was performed. It should be noted that the re-

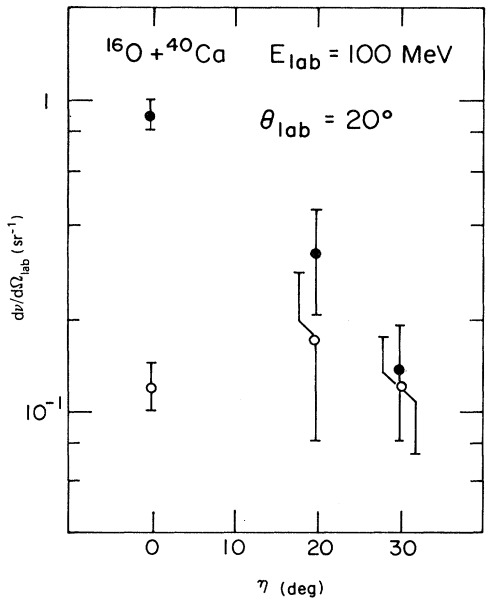


FIG. 19. The out-of-plane differential multiplicity at $\theta_{lab}=20°$ for alpha particles (filled circles) and protons (open circles) in $^{40}Ca(^{16}O,^{12}C)$ at 100 MeV. ($\eta$ is the out-of-plane angle.)

sults are not sensitive to the choice of this parameter. Changing the value of $\Delta\theta$ to 11° did not produce an appreciable change in the results.

## IV. RESULTS AND DISCUSSION

The analysis was done for PF charges of $Z=6-10$ in coincidence with neutrons, and $Z=6-8$ in coincidence with alpha particles and protons. The total kinetic energy TKE of both fragments was TKE=25–85 MeV for the 142 MeV experiments and TKE=20–60 MeV for the 100 and 102 MeV experiments. The lower energy limits were chosen to minimize the contribution from the C backing and the higher energy limits were set below the quasielastic peak.

### A. The singles data

In Fig. 6 we present the $Z$ distribution obtained from the different experiments. It is seen that oxygen and carbon were the dominant elements detected. It is also seen that at 100 MeV the ratio of oxygen to carbon yield increases with decreasing angle. The average $Q$ values obtained for all elements in the different measurements are given in Table III. The laboratory energy spectra in all experiments for C, N, and O are shown in Figs. 7 and 8 (the spectra were smoothed over a range of 2.5 MeV). The angular distribution was measured only for 100 MeV $^{16}O$ on $^{40}Ca$ and it is given in Fig. 5. The average slope of these spectra is the $\Delta\theta$ which was used for the coincidence analysis as described in Sec. III.

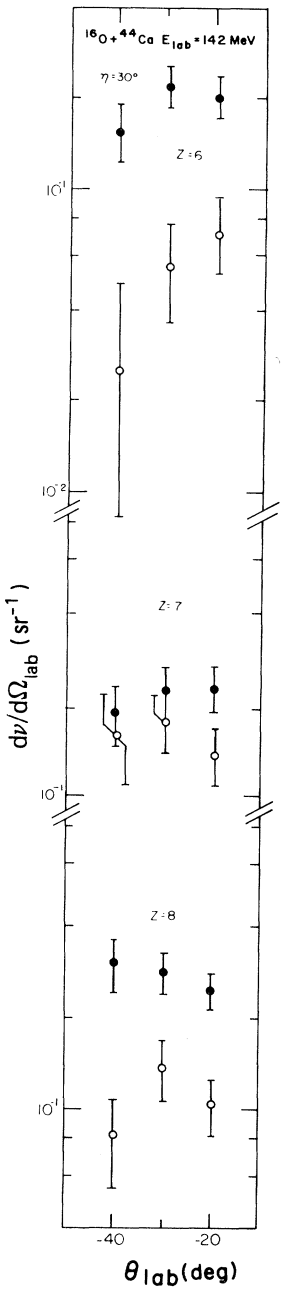


FIG. 20. The out-of-plane differential multiplicity for alpha particles (filled circles) and protons (open circles) for PF's from carbon to oxygen in $^{16}O + ^{44}Ca$ at 142 MeV. The out-of-plane angle is $\eta=30°$ and the measurements were taken at three in-plane laboratory angles $\theta_{lab}$.

### B. The coincidence data

Figure 9 shows the laboratory angular distribution of the neutrons (closed circles) in the $^{44}Ca$ experiments. The angular distribution of neutrons, alpha particles, and protons in the $^{48}Ca$ experiment is presented in Fig. 10. The sharply forward peaked distributions are similar to those observed by other workers.[10–19]

### 1. Neutrons

The reference neutron counters are PM 3 and PM $\bar{1}$ (see the lower part of Table II), which are located close to the TF and the PF directions, respectively. The projected laboratory angular distributions for neutrons are given in Figs. 9 and 10 as solid lines, the projected spectra from the TF alone are indicated in the figures as dotted-dashed lines. It is seen that the TF contribution is nearly isotropic in the laboratory system; it changes only by a factor of 2 between $-80°$ and $+80°$. This is due to the small velocity of the recoiling TF. The difference between the two lines represents the neutrons emitted from the PF, and it is seen that the forward peak of the distribution is due to emission from this fragment. Although the neutron multiplicity from the TF is about six times bigger than that of the PF (see Table IV), the emission from the latter dominates the distribution at forward angles. This is due to the high velocity of the PF which focuses the LP in the laboratory into a narrow cone centered around its direction. The importance of the HI angular distribution and the recoil correction is illustrated in Fig. 10 by the dashed line. This line is the projection from the reference counters on the other detectors assuming the HI angular distribution is isotropic in the center of mass. The difference between the dashed line and the solid line demonstrates the importance of taking into account the HI angular distribution in the analysis.

In Figs. 11—13, we show the measured spectra (closed circles) and the projected velocity spectra (open circles) of all the detectors. The good agreement for all six in-plane geometries supports our assumption of statistical emission. A small anisotropy is observed in the out-of-plane counters (PM 5 and PM $\bar{5}$) which may be due to fragment alignment. The relation between the anisotropy and the angular momentum transfer is not a simple one; the alignment can be destroyed by emission of an alpha particle which carries much of the angular momentum of the emitter. For this reason we did not attempt to obtain information on the angular-momentum transfer from the observed anisotropy.

The neutron spectra in the c.m. frame of the emitting fragment are shown in Fig. 14. The spectra are compatible with a Maxwellian distribution

$$\frac{d\sigma}{dE_n} \propto \sqrt{E_n}\exp(-E_n/T)\,, \tag{4.1}$$

with the values of $T$ given in Table III. However, these values of $T$ should not necessarily be identified with a nuclear "temperature." These words of caution apply in particular to the PF since its mass number and excitation energy (10—15 MeV) are too low to make the concept of a nuclear temperature a valid one. The difference in the slopes of the c.m. energy distributions between the TF and PF for the same systems (Fig. 14) does, therefore, not necessarily indicate a lack of energy equilibration between the two fragments. (Since the PF has a level density lower than that expected from the degenerate Fermi gas model it is to be expected that its excitation energy should be lower than given from the fragment mass ratio, i.e., its temperature $T$ should be *lower* than that of the TF, as indeed is seen in Fig. 14 and Table III.)

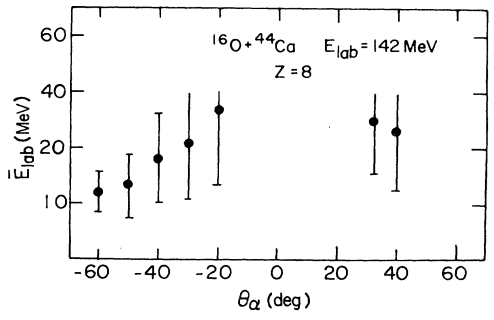


FIG. 21. Average laboratory energy for alpha particles in coincidence with oxygen versus the alpha detector laboratory angles in $^{16}O + ^{44}Ca$ at 142 MeV.

### 2. Alpha particles and protons

The laboratory angular distribution for alpha particles and protons in coincidence with C, N, and O are given in Figs. 15—18. They have a broad forward peak which is more pronounced for alpha particles and seems to be somewhat shifted to the negative angles, i.e., to the side of the beam where the TF is emitted. The out-of-plane data of alpha particles are shown in Figs. 19 and 20. (In these figures $\eta$ is the angle above the reaction plane, i.e., the angle between the line connecting the detector with the center of the target and the horizontal plane.) They exhibit an anisotropy which presumably is due to the alignment of the fragments. The proton data do not show such a strong anisotropy.

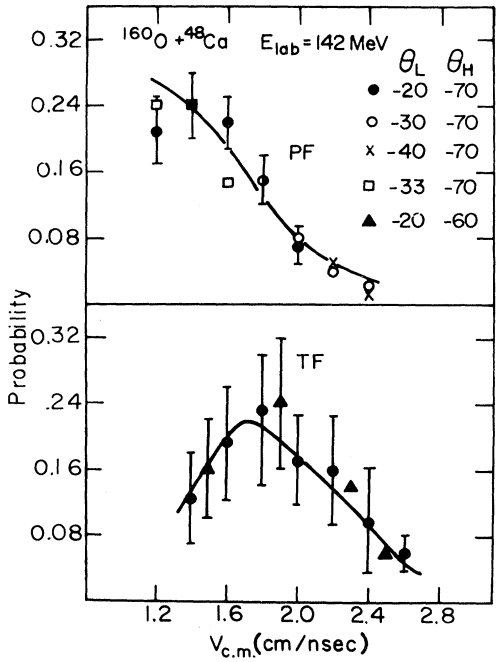


FIG. 22. The c.m. velocity distribution of alpha particles emitted by the PF and TF in the $^{16}O + ^{48}Ca$ at 142 MeV experiment. The data points were obtained using the reference counters as indicated in the figure (the sign convention for the angles is as in Fig. 14). The solid line is a fit to the data points using a Maxwellian distribution.

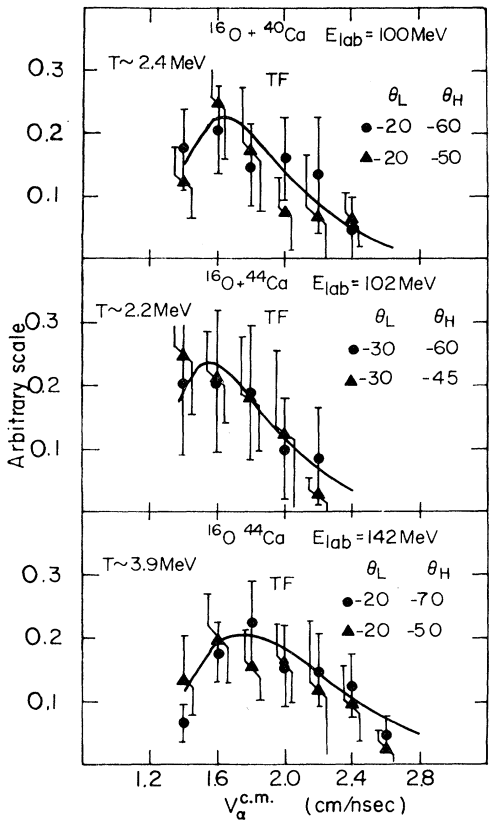


FIG. 23. The c.m. velocity distribution of alpha particles emitted by the TF in the 1st—3rd experiments. The data points were obtained using the reference counters as indicated in the figure (the sign convention for the angles is as in Fig. 9). The solid line is a fit to the data points using a Maxwellian distribution.

For alpha particles we cannot show a figure similar to Figs. 11—13 for two reasons: (1) the statistics were worse than for the neutrons; and (2) the lower and upper energy cutoffs for the alpha particles reduced their velocity range, and therefore the overlap of the regions, in the space of c.m. alpha velocity versus total kinetic energy, covered by the various detector geometries, is much reduced. An example of the average alpha energy in the laboratory energy versus angle is given in Fig. 21. Because of the limitations mentioned above we cannot reproduce the whole c.m. spectra (especially that of the PF) from the alpha spectra measured at just two reference angles. However, we took *all* detector angles and calculated from each of them *a segment* of the c.m. velocity spectrum. The contribution of alpha emission from the TF can be derived with reasonable accuracy (see Figs. 22 and 23), but those of the PF have large errors in most of the experiments and are plotted, in Fig. 22, only for $^{16}O+^{48}Ca$ at 142 MeV. The agreement between the overlapping regions shows that the reconstructed LP c.m. spectrum is consistent with our assumption of isotropic evaporation. However, the evidence for isotropic emission from the fragments is less convincing than in the case of neutron emission. The c.m. velocity spectra shown in Figs. 22 and 23 can be fitted by a shifted Maxwellian distribution,

$$\frac{d\sigma}{dv} \propto \frac{(\frac{1}{2}mv^2-B)^{1/2}}{v}\exp-(\tfrac{1}{2}mv^2-B)/T \qquad (4.2)$$

($v$ is the c.m. alpha velocity, and $B$ is the Coulomb shift parameter). The values of $T$ extracted from Fig. 22 are about 3.5 MeV for the TF and about 2.6 MeV for the PF with uncertainties of about 50%. The temperatures obtained from Fig. 23 by a least-square fit (the errors are about ±50%) are shown in the figure and they are in reasonable agreement with the neutron data. For protons the statistics are even poorer than for alpha particles but the total yield at each direction is in agreement with isotropic emission within the statistical errors (about 40—50 %).

### C. Multiplicities of LP, excitation energy, and angular momentum

Table IV shows the average multiplicities and energies in the c.m. for the light particles. The average excitation energy $\bar{E}^*$ for each fragment can be deduced from the equation

$$\bar{E}^*_j = \sum_i \bar{\nu}^i_j(\bar{E}^i_j + B^i_j) + S\ , \qquad (4.3)$$

where $i$ stands for the LP index (n, p, $\alpha$, and gamma), and $j$ is the emitter index (TF or PF). $S$ is the energy carried away by the gammas and it was assumed to be equal to half of the threshold energy for LP emission. The average total excitation energies deduced from these multiplicities are given in Table III and they are in agreement with the measured average $Q$ value. The temperatures deduced from the TF c.m. spectra can also give us some information on the excitation energies using the formula

$$E^* = aT^2\ , \qquad (4.4)$$

where $a$ is the level density parameter. It is seen that the excitation energies obtained from (4.4) by using $a = A/10$ $MeV^{-1}$ are consistent with the excitation energies from Eq. (4.3); see Table III.

Comparing the LP multiplicities in the different experiments (Table IV) we observe the following features: (a) the multiplicities increase with the bombarding energy in agreement with the additional excitation energy available; (b) the ratio of neutron to alpha multiplicities of the TF changes drastically from $^{44}Ca$ to $^{48}Ca$ target, but (c) the alpha multiplicity is the same for both targets in the 142 MeV experiments. This may reflect the possibility that we are close to the yrast line, and as a result the alpha emission is enhanced. The multiplicities of all LP emitted from the PF are essentially the same for the $^{44}Ca$ and $^{48}Ca$ at 142 MeV, which is reasonable since the excitation energy of the PF is almost unaffected by changing the target mass. Finally, it should be emphasized that the multiplicities and the excitation energies deduced from them are upper limits, since the LP are assumed to be emitted isotropically in the rest frame of the fragment and our results show that there is a certain amount of anisotropy (which may depend on the specific LP and on the bombarding energy).

## V. SUMMARY

We conclude, mainly on the basis of the neutron results, that our data are consistent with the assumption of isotropic emission of the LP from the fully accelerated fragments. The laboratory angular distribution of the LP has a strong forward peak. We have shown that this forward peak originates from LP emission from the PF, and is essentially due to the strong focusing of the LP in the laboratory system and to the exponential dependence of the PF differential cross section, the recoil of PF by LP emission. Although its multiplicity is small, the LP emission from the PF dominates the angular distribution of the LP in the laboratory.

---

*Present address: Lawrence Berkeley Laboratory, Building 88, Berkeley, CA 94720.

†Present address: Nuclear Research Center Democritos, Athens, Greece.

‡Present address: Fachbereich Physik, Phillipps Universitat, Marburg, Federal Republic of Germany.

[1]Y. Eyal, A. Gavron, I. Tserruya, Z. Fraenkel, Y. Eisen, S. Wald, R. Bass, G. R. Gould, G. Kreyling, R. Renfordt, K. Stelzer, R. Zitzmann, A. Gobbi, U. Lynen, H. Stelzer, I. Rode, and R. Bock, Phys. Rev. Lett. 41, 625 (1978).

[2]Y. Eyal, A. Gavron, I. Tserruya, Z. Fraenkel, Y. Eisen, S. Wald, R. Bass, G. R. Gould, G. Kreyling, R. Renfordt, K. Stelzer, R. Zitzmann, A. Gobbi, U. Lynen, H. Stelzer, I. Rode, and R. Bock, Phys. Rev. C 21, 1377 (1980).

[3]D. Hilscher, J. R. Birkelund, A. D. Hoover, W. U. Schröder, W. W. Wilcke, J. R. Huizenga, A. C. Mignerey, K. L. Wolf, H. F. Breuer, and V. E. Viola, Phys. Rev. C 20, 576 (1979).

[4]B. Tamain, R. Chechik, H. Fuchs, H. Hanappe, M. Morjean, C. Ngô, J. Péter, M. Dakowski, B. Lucas, C. Mazur, M. Ribrag, and C. Signarbieux, Nucl. Phys. A330, 253 (1979).

[5]M. Dakowski, R. Chechik, H. Fuchs, F. Hanappe, B. Lucas, C. Mazur, M. Morjean, J. Péter, M. Ribrag, C. Signarbieux, and B. Tamain, Z. Phys. A 294, 289 (1980).

[6]C. R. Gould, R. Bass, J. V. Czarnecki, V. Hartmann, K. Stelzer, R. Zitzmann, and Y. Eyal, Z. Phys. A 284, 253 (1978).

[7]F. Plasil, R. L. Ferguson, H. C. Britt, R. H. Stokes, B. H. Erkkila, P. D. Goldstone, M. Blann, and H. H. Gutbrod, Phys. Rev. Lett. 40, 1164 (1978).

[8]D. Guerreau and J. Galin, in *Proceedings of the Symposium on Heavy-Ion Physics from 10 to 200 MeV/AMU,* edited by J. Barrette and P. D. Bond, BNL, Upton, New York, 1979.

[9]I. Tserruya, A. Breskin, Z. Fraenkel, S. Wald, R. Bock, M. Dakowski, A. Gobbi, H. Sann, R. Bass, G. Kreyling, R. Renfordt, K. Stelzer, and U. Arlt, Phys. Rev. Lett. 47, 16 (1981); Phys. Rev. C 26, 2509 (1982).

[10]J. W. Harris, T. M. Cormier, D. F. Geesman, L. L. Lee, Jr., R. L. McGrath, and J. P. Wurm, Phys. Rev. Lett. 38, 1460 (1977).

[11]J. W. Harris, *Proceedings of the International Conference on Nuclear Structure, Tokyo, 1977* (International Academic, Tokyo, 1977), Vol. I, p. 698.

[12]H. Ho, R. Albrecht, D. Dünnweber, G. Graw, S. G. Steadman, J. P. Wurm, D. Disdier, V. Rauch, and F. Scheibling, Z. Phys. A 283, 237 (1977).

[13]R. K. Bhowmik, E. C. Pollaco, N. E. Sanderson, J. B. A. England, and G. C. Morrison, Phys. Lett. 80B, 41 (1978); Phys. Rev. Lett. 43, 619 (1979).

[14]R. Billerey, C. Cerutti, A. Chevarier, N. Chevarier, B. Cheynis, and A. Demeyer, Z. Phys. A 292, 293 (1979).

[15]C. K. Gelbke, Phys. Lett. 71B, 83 (1977).

[16]M. Sasagase, M. Sato, S. Hanashima, K. Furuno, Y. Tagishi, Y. Nagashima, S. M. Lee, and T. Mikumo, *Proceedings of the International Symposium on Continuum Spectra of Heavy Ion Reactions, San Antonio, 1979* (Harwood Academic, New York, 1980), p. 33.

[17]T. Shimoda, M. Ishihara, H. Kamitsubo, T. Motobayashi, and T. Fukuda, in Proceedings of the IPCR Symposium on Macroscopic Features of Heavy Ion Collisions and Preequilibrium Process, Hakone, 1977, IPCR Cyclotron Report Suppl. 6, p. 83.

[18]A. Gamp. J. C. Jacmart, N. Poffé, H. Doubre, J. C. Roynette, and J. Wilczynski, Phys. Lett. 74B, 215 (1978).

[19]H. Gemmeke, P. Netter, Ax. Richter, L. Lassen, S. Lewandowski, W. Lücking, and R. Schreck, Phys. Lett. 97B, 213 (1980).

[20]A. Gamp, M. Clover, C. Egelhaaf, H. Fuchs, B. Gebauer, H. Homeyer, and J. C. Jacmart, Z. Phys. A 300, 1 (1981).

[21]M. B. Tsang, W. G. Lynch, R. J. Puigh, R. Vandenbosch, and A. G. Seamster, Phys. Rev. C 23, 1560 (1981).

[22]M. Bini, C. K. Gelbke, D. K. Scott, T. J. M. Symons, P. Doll, D. L. Hendrie, J. L. Laville, J. Mahoney, M. C. Mermaz, C. Olmer, K. Van Bibber, and H. M. Wieman, Phys. Rev. C 22, 1945 (1980).

[23]G. R. Young, R. L. Ferguson, A. Gavron, D. C. Hensley, F. E. Obershain, F. Plasil, A. H. Snell, M. P. Webb, C. F. Maguire, and G. A. Petitt, Phys. Rev. Lett. 45, 1389 (1980).

[24]A. Gavron, R. L. Ferguson, F. E. Obershain, F. Plasil, G. R. Young, G. A. Petitt, K. A. Geoffroy, D. G. Sarantites, and C. F. Maguire, Phys. Rev. Lett. 46, 8 (1981).

[25]S. Wald, I. Tserruya, Z. Fraenkel, G. Doukellis, H. Gemmeke, and H. L. Harney, Phys. Rev. C 25, 1118 (1982).

[26]M. M. Fowler and R. C. Jared, Nucl. Instrum. Methods 124, 341 (1975).

[27]M. Drosg, Nucl. Instrum. Methods 105, 582 (1072).

[28]S. Wald, I. Tserruya, and Z. Fraenkel, Nucl. Instrum. Methods 206, 119 (1983).

[29]V. Strutinsky, Z. Phys. A 286, 77 (1977).